Improvements to the AMOEBA Force Field by Introducing Anisotropic Atomic Polarizability of the Water Molecule

Akshaya K. Das[1,2*], Omar N. Demerdash[1,2*], and Teresa Head-Gordon[1-4†]

[1]Pitzer Center for Theoretical Chemistry, [2]Department of Chemistry, [3]Department of Bioengineering, [4]Department of Chemical and Biomolecular Engineering, University of California, Berkeley CA 94720

In this work we have developed an anisotropic polarizable model for the AMOEBA force field that is derived from electrostatic fitting on a gas phase water molecule as the primary approach to improve the many-body polarization model. We validate our approach using small to large water cluster benchmark data sets, ambient liquid water properties, and through comparisons to a variational energy decomposition analysis breakdown of molecular interactions for water and water-ion trimer systems. We find that the accounting of anisotropy for a single water molecule demonstrably improves the description of the many-body polarization energy in all cases. This study provides a proof of principle for extending our protocol for developing a general purpose anisotropic force field for other biological and material functional groups to better describe complex and asymmetric environments for which accurate polarization models are most needed.

Keywords: Anistropic polarization, AMOEBA force field, EDA analysis

*both authors contributed equally to this work
†corresponding author: thg@berkeley.edu

INTRODUCTION

Molecular dynamic (MD) simulations are widely used to study the physical properties of large and complex systems such as associated liquids, proteins and enzymes, nucleic acids, lipid membranes, as well as non-biological materials such as polymers, metal organic frameworks, zeolites, and diverse interfaces and surfaces.[1-10] The success of the MD approach relies inherently on the accuracy of the potential energy surface and the ability to sample phase space until convergence of properties of interest are reached.[11] One of the main advantages of empirical interatomic potentials is that they are computationally tractable for simulating large systems on long time scales[6, 12-13], since they use a simple pairwise additive approximation to capture strong intermolecular interactions such as permanent electrostatics.[11] Most conventional force fields rely on fixed partial charges on the atomic nuclei under Ewald conditions to correctly capture the asymptotic regime of permanent electrostatics. More sophisticated electrostatic interactions such as higher order multipoles and charge penetration have been developed to improve upon the standard two-body approximation for intermediate and short-range separations. However, pairwise additivity begins to breakdown due to neglect of inherently electronic response effects such as many-body polarization, charge transfer, and higher order dispersion and Pauli repulsion.

Beyond permanent electrostatics, explicit many-body polarization is the next consideration for capturing strong interactions (that decay with a $1/r^n$ dependence) and improving both the qualitative and quantitative description of empirical potential energy surfaces. In recent years, several force fields have been developed that are centered around such advanced many-body interactions including Sum of Interactions Between Fragments Ab initio computed (SIBFA)[14], the CHARMM Drude model[15], Chemical Potential Equalization (CPE)[16], Gaussian Electrostatic Model (GEM)[17-18], and Atomic Multipole Optimized Energetics for Biomolecular Applications (AMOEBA)[19-21]. Although the incorporation of many-body physics increases the computational cost of force fields significantly, advanced software implementations and hardware resources[22-23] and the advent of new algorithms that mitigate their cost[23-25], makes it far more tractable to incorporate and assess many-body potentials and their performance in various chemical and biochemical contexts. While there are many examples in which advanced potential energy models succeed due to their improved physics[11, 26], there are also emerging failures in which they are outperformed by their fixed charge counterparts. For example, in the case of blind prediction in the Statistical Assessment of the Modeling of Proteins and Ligands (SAMPL) exercises[27-29], it has been shown that the fixed-point-charge models are often

as or more accurate for hydration free energies and guest-host ligand binding than are the more sophisticated polarizable counterparts[30].

For any force field, the underlying source of their errors resides in the choice of functional form and formulations of their parameters for explicitly represented interactions (such as exchange repulsion, permanent electrostatics, and polarization), a reliance on cancellation of errors by ignoring other terms (such as charge transfer and/or charge penetration), and the assumption that interactions can be broken down into piecewise functions. In order to understand these failures, and therefore to correct force field deficiencies, we need better tools to interrogate the individual contributions of many-body intermolecular interactions. One approach that we and others have focused on is the piecewise decomposition of an ab initio potential energy surface[31-36], for example using symmetry adapted perturbation theory (SAPT)[37-38] or variational energy decomposition analysis (EDA) based on absolutely-localized molecular orbitals (ALMO-EDA))[39-40] methods. Although both SAPT and ALMO-EDA approaches agree in the asymptotic range, they do differ in their description of intermolecular interactions in the so-called compressed region where there is more entanglement of the individual terms. This "non-uniqueness" issue has been discussed in detail elsewhere[41-44]. Our view is the EDA schemes will ultimately be validated when they can demonstrably and systematically guide force field development over the current practice of hand-tuning of parameters.

In previous work we have used ALMO-EDA to decompose the ωB97X-V/def2-QZVPPD[45-46] potential energy to analyze the piecewise decomposition of the AMOEBA force field on simple water and water-ions dimer[42] and trimer systems[26]. Not surprisingly, given the correct functional forms at long range, AMOEBA is well formulated in its decomposition in the asymptotic region. However it can differ with the ALMO-EDA terms on both sides of the equilibrium geometry at short range due to incorrectly formulated exchange-repulsion, electrostatics, dispersion, and polarization, and arbitrary accounting of the missing charge penetration and charge transfer terms. For example, AMOEBA uses a functional form for the many-body polarization of point inducible dipoles that are damped at short range with a Thole/Applequist-like model, and parameterized using a single scalar for the isotropic atomic polarizability.[19, 47] As we will show again here, this gives rise to the often cited overestimate of AMOEBA's polarization energy.[6, 21, 26, 47-48]

In this work we introduce anisotropic polarizability parameterized on a single water molecule as the primary approach to improve the many-body polarization model for the AMOEBA force field. We validate our approach for small to large water cluster data at equilibrium and for distorted geometries, for bulk water, and through comparisons of the ALMO-EDA breakdown for water and

water-ion trimer systems, since metal ions play such an important role in biological systems[49-50], and the fact that cations and anions will show a large range in anisotropic response to the electrostatic field. We find that anisotropic polarization greatly improves the description of the many-body polarization energy of all examined systems, providing a proof of principle in extending our protocol for the anisotropic AMOEBA model to other protein functional groups and materials.

THEORY AND METHODS

Theory. Many-body polarization is explicitly incorporated in the AMOEBA model by induced dipoles at polarizable sites located on each atomic center.[47] The induced dipoles $\boldsymbol{\mu}_i^{\mathrm{ind}}$ at a polarizable site *i* with polarizability α_i is expressed as

$$\boldsymbol{\mu}_i^{\mathrm{ind}} = \alpha_i \left(\sum_j \boldsymbol{T}_{ij}^{\mathrm{d}} \boldsymbol{M}_j + \sum_{j \neq i} \boldsymbol{T}_{ij}^{\mathrm{d-d}} \boldsymbol{\mu}_j^{\mathrm{ind}} \right) \tag{1}$$

Where $\boldsymbol{M}_j$ and $\boldsymbol{T}_{ij}^{\mathrm{d}}$ are the permanent multipoles and multipole-multipole interaction tensor, respectively, and the $\boldsymbol{T}_{ij}^{\mathrm{d-d}}$ are the Thole damped[48] Cartesian interaction tensors between induced dipoles of two polarizable sites *i* and *j*.[19, 51]. The Thole damping of the pairwise multipole interactions are carried out by using damping function[47]

$$\rho = \frac{3a}{4\pi} \exp\left(-a \frac{r_{ij}^3}{(a_i a_j)^{\frac{1}{2}}} \right) \tag{2}$$

where r_{ij} is the distance between atomic sites *i* and *j* and *a* is a dimensionless width parameter that effectively controls the strength of the damping[52].

The first term in parentheses on the right hand side of the equation (1) is the direct polarization electric field $\boldsymbol{E}_i$ of induced dipoles by the permanent multipoles, and therefore Eq. (1) can be rewritten as

$$\alpha_i^{-1} \boldsymbol{\mu}_i^{\mathrm{ind}} - \sum_{j \neq i} \boldsymbol{T}_{ij}^{\mathrm{d-d}} \boldsymbol{\mu}_j^{\mathrm{ind}} = \boldsymbol{E}_i \tag{3}$$

or more generally as

$$\begin{pmatrix} \alpha_1^{-1} & -\boldsymbol{T}_{12}^{\mathrm{d-d}} & \dots & -\boldsymbol{T}_{1N}^{\mathrm{d-d}} \\ -\boldsymbol{T}_{21}^{\mathrm{d-d}} & \alpha_2^{-1} & \dots & -\boldsymbol{T}_{2N}^{\mathrm{d-d}} \\ \vdots & \vdots & \ddots & \vdots \\ -\boldsymbol{T}_{N1}^{\mathrm{d-d}} & -\boldsymbol{T}_{N2}^{\mathrm{d-d}} & \dots & \alpha_N^{-1} \end{pmatrix} \begin{pmatrix} \boldsymbol{\mu}_1^{\mathrm{ind}} \\ \boldsymbol{\mu}_2^{\mathrm{ind}} \\ \vdots \\ \boldsymbol{\mu}_N^{\mathrm{ind}} \end{pmatrix} = \begin{pmatrix} \boldsymbol{E}_1 \\ \boldsymbol{E}_2 \\ \vdots \\ \boldsymbol{E}_N \end{pmatrix} \tag{4}$$

In Eq. (4) the diagonal blocks are the inverse of the polarizability, and the AMOEBA model assumes the following simple isotropic form

$$\alpha_i^{-1} = \begin{pmatrix} \alpha_{i,xx}^{-1} & 0 & 0 \\ 0 & \alpha_{i,yy}^{-1} & 0 \\ 0 & 0 & \alpha_{i,zz}^{-1} \end{pmatrix} \tag{5}$$

Here we introduce anisotropic polarizability to improve the many-body polarization model for the AMOEBA force field by representing the atomic polarizability as a rank two tensor.

$$\alpha_i^{-1} = \begin{pmatrix} \alpha_{i,xx}^{-1} & \alpha_{i,xy}^{-1} & \alpha_{i,xz}^{-1} \\ \alpha_{i,yx}^{-1} & \alpha_{i,yy}^{-1} & \alpha_{i,yz}^{-1} \\ \alpha_{i,zx}^{-1} & \alpha_{i,zy}^{-1} & \alpha_{i,zz}^{-1} \end{pmatrix} \tag{6}$$

Parameterization. We took the following design strategy in the parameterization of the distributed anisotropic atomic polarizabilities for a water molecule. Atomic polarizabilities for the water molecule were obtained using the techniques of Stone, Misquitta, and co-workers using the CamCASP[53] and ORIENT[54] suite of programs. First, distributed, *ab initio*-derived polarizabilities were obtained using the method of Misquitta and Stone[55-56], whereby a frequency-dependent point charge perturbation is applied to a molecule at regular distance intervals outside the molecular surface. Zero frequency corresponds to the static polarizability, and is the focus of this work, while non-zero frequencies can be used to obtain the coefficients (C_6, C_8, C_{10}, etc.) for dispersion. These calculations were performed at the PBE0/aug-cc-pVTZ level of theory in the CamCASP suite, which in turn used NWChem[57] for the DFT calculation. After this step, the polarizabilties are localized to derive atomic polarizabilties using the Williams-Stone-Misquitta (WSM) technique[58] implemented in the ORIENT program.

In contrast to Thole/Appelquist models like AMOEBA, the Misquitta/Stone regime of polarization assumes no intramolecular polarization. In AMOEBA, there is no contribution to intramolecular polarization from the permanent multipoles, but there is among the induced dipoles within a molecule or polarization group. To account for the presence of intramolecular polarization in the parameterization of standard AMOEBA, the contribution of Thole-damped polarization is subtracted from the multipoles calculated from distributed multipole analysis (DMA), yielding the polarization-free permanent multipoles used in the AMOEBA force field. Therefore, to be compatible with the Misquitta/Stone model, our anisotropic model for water introduces no intramolecular polarization either from the permanent multipoles or among the induced dipoles. Hence the permanent multipoles must be re-derived to account for the lack of intramolecular polarization. In order to make

minimal change to the existing AMOEBA 2003 force field parameters[47], we fixed both atomic monopoles and dipoles, and allowed atomic quadrupoles to optimize with respect to the *ab initio* electrostatic potential (ESP) on grid points outside the van der Waals surface of the water molecule. To be consistent with AMOEBA, the reference *ab initio* ESP was obtained at the level of MP2/aug-cc-pVTZ using Gaussian09 program[59]. The force field parameters for the anions F^- and Br^- are taken from AMOEBA09[19], and all other parameters are taken from the AMOEBAPro13 force field[20].

Analysis. We have evaluated different water properties including small to large water cluster data sets, basic bulk water properties, and for ion-water systems. For the latter systems, direct comparison was made with the breakdown of the *ab initio* energy, using the energy decomposition analysis[31] based on absolutely localized molecular orbitals (ALMO-EDA) method[39-40, 60]. This allows us to separate the total interaction energy into individual contributions from permanent electrostatics (E_{elec}), Pauli repulsion (E_{pauli}), dispersion (E_{disp}), polarization (E_{pol}), and charge transfer (E_{ct}):

$$E_{\mathrm{int}} = E_{\mathrm{elec}} + E_{\mathrm{pauli}} + E_{\mathrm{disp}} + E_{\mathrm{pol}} + E_{\mathrm{ct}} \quad (7)$$

Derivation of the each of the individual energy components are described elsewhere[39-40, 42, 60-61]. All the ALMO-EDA calculations are performed at the level of a hybrid generalized gradient approximation (hybrid GGA) functional which includes the VV10 non-local correlation functional for dispersion correction, ωB97X-V/def2-QZVPPD[45-46]. Although based on DFT, the ωB97X-V/def2-QZVPPD functional and basis set[45-46] has been validated against high quality CCSD(T)/CBS calculations on multiple benchmark data sets, and hence its total energy is considered to be highly reliable with ~0.5 kcal/mol error for all systems except Mg^{2+}-H_2O systems at long range; we return to this point later. All ALMO-EDA calculations were performed using the Q-chem package[62].

For assessing whether the molecular interactions of the anisotropic AMOEBA model yield better agreement with the ALMO-EDA result, energy calculations as a function of intermolecular distance, d, were performed for water and water-ion trimers, starting from the equilibrium optimized structures (always defined as $d = 0$ on the distance axis) using ωB97X-V/def2-QZVPPD. Depending on the system, different types of intermolecular distance scans were performed that can result in a more compressed configuration ($d < 0$) or stretched to distances that reach the asymptotic regime ($d > 0$). For the water trimer, one of the water molecules is displaced from the centroid of the triangle formed by the three water oxygens (Fig. 1a). In the case of the $(H_2O)_2M^{n+}$ systems, the distance scans were performed along the M-O distances by displacing two water molecules simultaneously from the metal center (Fig. 1b). For the $(H_2O)_2X^{n-}$ systems, the scanned coordinate is similar to water-trimer system, where the anion is displaced from the centroid of the triangle formed by the three heavy atoms

(Fig. 1c). For the two cation and one water systems, the initial geometry was prepared by placing two metal ions at a distance corresponding to the equilibrium distance in the $(H_2O)M^{n+}$ dimer, with the angle between the M-O and the bisector of the H_2O molecule fixed at 45°; distance scans were performed by displacing two metal ions simultaneously along the M-O bond direction (Fig. 1d). Similarly, for systems with two anions, the initial geometry was prepared by considering the equilibrium geometry of the $(H_2O)X^{n-}$ dimer and the second ion was placed by a reflection about the X^--O-H angle. The two halogen ions were moved simultaneously along the O-X distance for the distance scan (Fig. 1e).

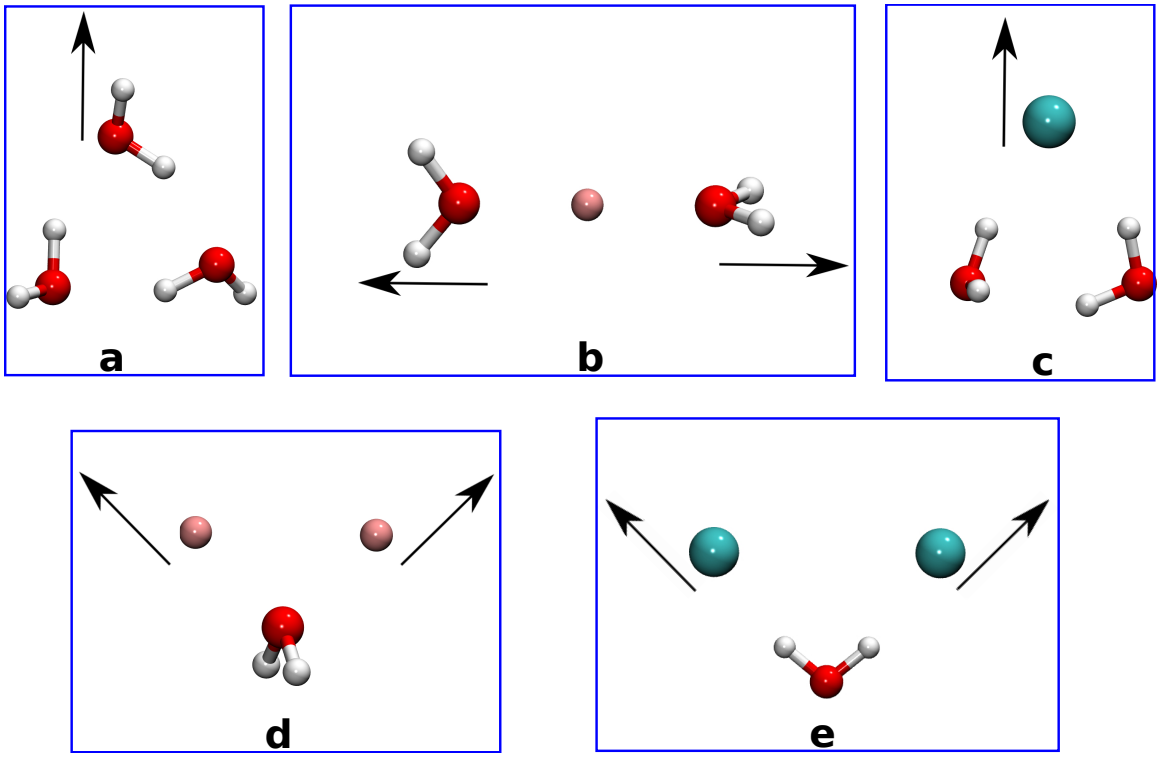

Figure 1. *Definition of the distance scans performed for the trimer different systems.* Arrows represents the scanned directions. (a) water trimer, (b) $(H_2O)_2M^{n+}$, (c) $(H_2O)_2\ X^{n-}$, (d) $H_2O(M^{n+})_2$ and (e) $H_2O(X^{n-})_2$.

RESULTS

Table 1 details the final atomic multipoles and polarizabilities for the new anisotropic AMOEBA (aniso-AMOEBA) model. Table 2 provides the molecular properties of the gas phase water molecule that result from the anisotropic water model, which is also compared to the same calculated properties of the previous AMOEBA03[47] and AMOEBA14[63] models, *ab initio* calculations, and experiment. It is interesting to note that the AMOEBA03 model was fit to the equilibrium water dimer properties from *ab initio* calculations as evident from Table 3 whereas the AMOEBA14 model focused on better

reproduction of condensed phase bulk properties and does not perform as well on the water dimer as a result. Overall aniso-AMOEBA performs as well as AMOEBA03 on the water dimer at equilibrium.

Table 1. *Aniso-AMOEBA model parameters for the water molecule*. The charges and dipole parameters for oxygen and hydrogen are the same as the original AMOEBA 2003[47] water model.

Multipoles	Oxygen	Hydrogen	**Polarizability**	Oxygen	Hydrogen
q	-0.51966	0.25983	α_{XX}	0.9412	0.2687
μ_Z	0.14279	-0.03859	α_{XY}	-0.0007	-0.0002
μ_X	N/A	-0.05818	α_{XZ}	-0.0061	0.0938
Q_{XX}	0.56803	-0.01730	α_{YX}	-0.0007	-0.0002
Q_{YY}	-0.65906	-0.07631	α_{YY}	0.9148	0.1941
Q_{XZ}	N/A	0.00007	α_{YZ}	-0.0000	0.0005
Q_{ZZ}	0.09103	0.09361	α_{ZX}	-0.0061	0.0938
			α_{ZY}	-0.0000	0.0005
			α_{ZZ}	0.9417	0.2224

Table 2. *Multipole and polarization properties for gas phase water molecule for aniso-AMOEBA compared to previous AMOEBA03[47] and AMOEBA14[63]*. Comparison is made to published experimental values.

	AMOEBA03	**AMOEBA14**	**Aniso-AMOEBA**	**Experiment**
Dipole d_z (Debye)	1.771	1.808	1.771	1.855[a]
Quadrupole (Debye·Å)				
Q_{xx}	2.502	2.626	2.689	2.630[b]
Q_{yy}	-2.168	-2.178	-2.408	-2.500[b]
Q_{zz}	-0.334	-0.045	-0.281	-0.130[b]
Polarizability ($Å^2 \cdot s^4 \cdot kg^{-1}$)				
α_{xx}	1.672	1.767	1.577	1.528[c]
α_{yy}	1.225	1.308	1.232	1.412[c]
α_{zz}	1.328	1.420	1.391	1.468[c]

[a] Reference [64]. [b] Reference [65]. [c] Reference [66].

Table 3. *Dimer equilibrium properties for AMOEBA03, AMOEBA14, and aniso-AMOEBA compared to ab initio calculations and experiment.* Dissociation energy, D_e (kcal/mol), O-O distance (Å), α (angle between O-O vector and O_{donor}-H_{donor} vector, degrees), β (angle between O-O vector and plane of acceptor molecule, degrees), total dipole moment (μ_{tot}, Debye).

Property	**AMOEBA03**	**AMOEBA14**	**Aniso-AMOEBA**	***ab Initio***	**Experiment**
D_e	4.96	4.64	5.35	4.98[c]	5.44±0.7[a]
r_{O-O}	2.892	2.908	2.896	2.907[c]	2.976[b]
α	4.18	4.41	2.93	4.18[c]	-1±10[b]
β	57.2	64.9	60.5	55.6[d]	57±10[b]
μ_{tot}	2.54	2.20	2.57	2.76[e]	2.643[b]

[a] Reference [67]. [b] Reference [68]. [c] Reference [69]. [d] Reference [70]. [e] Reference [71]

Figure 2 provides the intermolecular energy for the water trimer along the scanned coordinates for aniso-AMOEBA and AMOEBA03 compared to ALMO-EDA. Including atomic anisotropic polarizability in the water molecule improves the intermolecular polarization energy appreciably compared to the isotropic AMOEBA03 model across all distances (Fig. 2a). The polarization energy around the equilibrium distance using aniso-AMOEBA is –23.0 kJ/mol, which agrees well with the ALMO-EDA value of –21.6 kJ/mol, while the AMOEBA03 model overestimates the polarization energy by ~4.5 kJ/mol. Fig. 2b and 2c show that there is improved agreement using aniso-AMOEBA for the 2-body polarization in the compressed region. We mention at this point that the ALMO-EDA is able to rigorously decouple polarization from charge transfer (which are lumped together in the 'induction' term of SAPT EDA's), thereby allowing us to consider that contribution directly. Although charge transfer is not accounted for in the AMOEBA model, it is evident that the 3-body polarization model captures the ALMO-EDA polarization and charge transfer interactions almost perfectly throughout the distance scan. The corresponding total interaction energy of the water trimer using the AMOEBA03 force field is underbound throughout the scanned coordinate compared to ALMO-EDA, whereas the aniso-AMOEBA interaction energy matches well due to the improvement in polarization energies, given that the permanent electrostatics have changed negligibly (Fig. 2d).

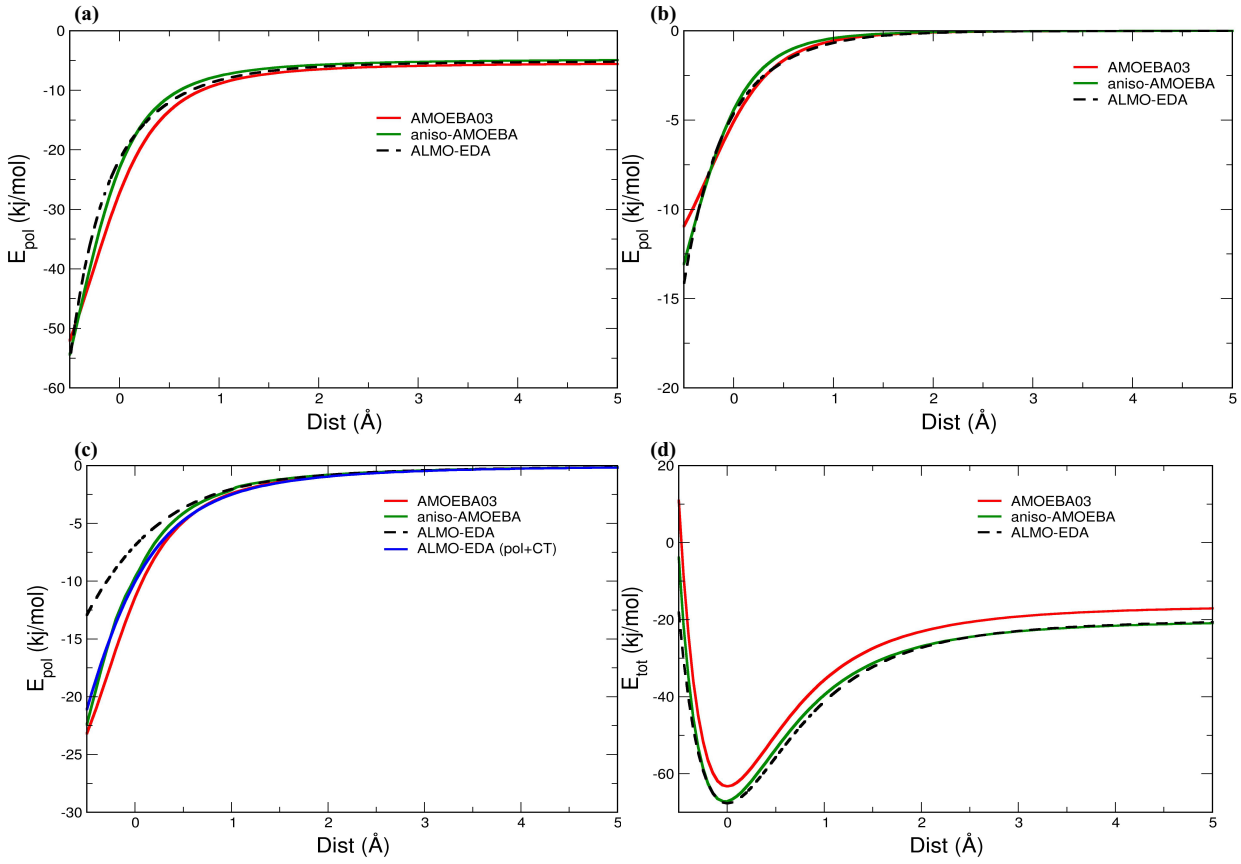

Figure 2. *Improvements in polarization for the AMOEBA model upon introduction of atomic anisotropic polarizability when compared to ALMO-EDA for the water trimer.* (a) Total polarization energy, (b) 2-body polarization, (c) 3-body polarization compared to EDA polarization with and without charge transfer, and (d) total interaction energy.

To further test the quality of intermolecular interactions for water clusters, we computed the energies using the aniso-AMOEBA model for data sets composed of small to large water cluster binding energies at equilibrium and distorted geometries, and compared it to the AMOEBA03 and AMOEBA14 water model and to *ab initio* reference calculations (Table S1). We find that the mean absolute deviations (MADs) for the small clusters is within chemical accuracy for AMOEBA14 and aniso-AMOEBA (0.39 vs. 0.62 kcal/mol, respectively), however the aniso-AMOEBA model provides a much smaller error in binding energies for water clusters containing more than 10 waters, yielding deviations from ab initio values of 2.95 kcal/mol versus the 7.97 kcal/mole error for the AMOEBA14 water model. Overall, the AMOEBA03 model has larger error on the smaller and larger clusters compared to aniso-AMOEBA, with MAD of 0.83 and 3.29 kcal/mol, respectively. To further test larger clusters distorted from equilibrium, we computed the polarization energy for 50 different water pentamers drawn from a 50 ps MD simulation at 298 K. The correlation in the polarization energy between ALMO-EDA, aniso-AMOEBA and standard AMOEBA03 is shown in Figure 3. From the correlation plot, it is clear that the aniso-AMOEBA model correlates much better with the ALMO-EDA polarization energy (RMSD = 4.1 kJ/mol) compared to the isotropic AMOEBA03 model (RMSD =12.5 kJ/mol).

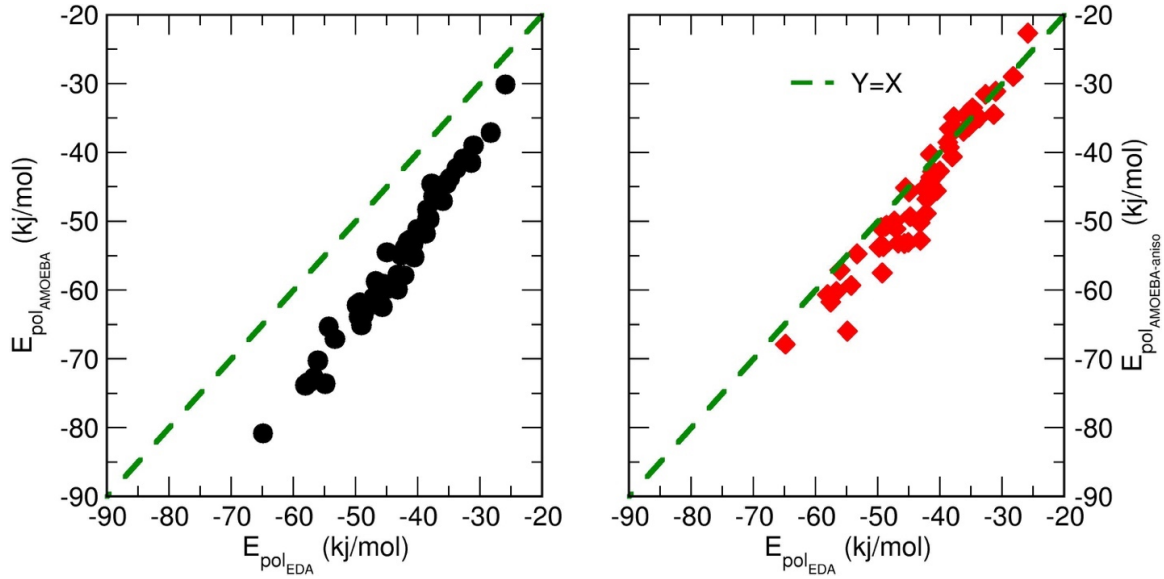

Figure 3. *Correlation of the polarization energy for water pentamers obtained from ALMO-EDA with AMOEBA03 (left, black symbols) and aniso-AMOEBA (right, red symbols).* 50 different water pentamer

configurations were extracted from a MD simulation for the ALMO-EDA analysis. The green dashed line represents the Y=X line for the force field vs. ab initio polarization energy.

Overall, introducing anisotropy as a single water molecule quantity translates into a cluster water model that shows improvement over both the original AMOEBA03 and the very different AMOEBA14 model that uses Force Balance for fitting to both QM and condensed phase data. We have implemented forces into the TINKER package that accounts for anisotropic polarization in order to calculate some basic bulk water properties to confirm the outcome from the water cluster data. Figure 4 shows the radial distribution functions in which it is evident that there is noticeable improvement in bulk water structure using the aniso-AMOEBA model compared to AMOEBA03. While AMOEBA03 model was fit to the ambient experimental density and enthalpy of vaporization, by contrast the aniso-AMOEBA still yields excellent agreement of 1.0 g/cc and 10.40 kcal/mole for these quantities, respectively.

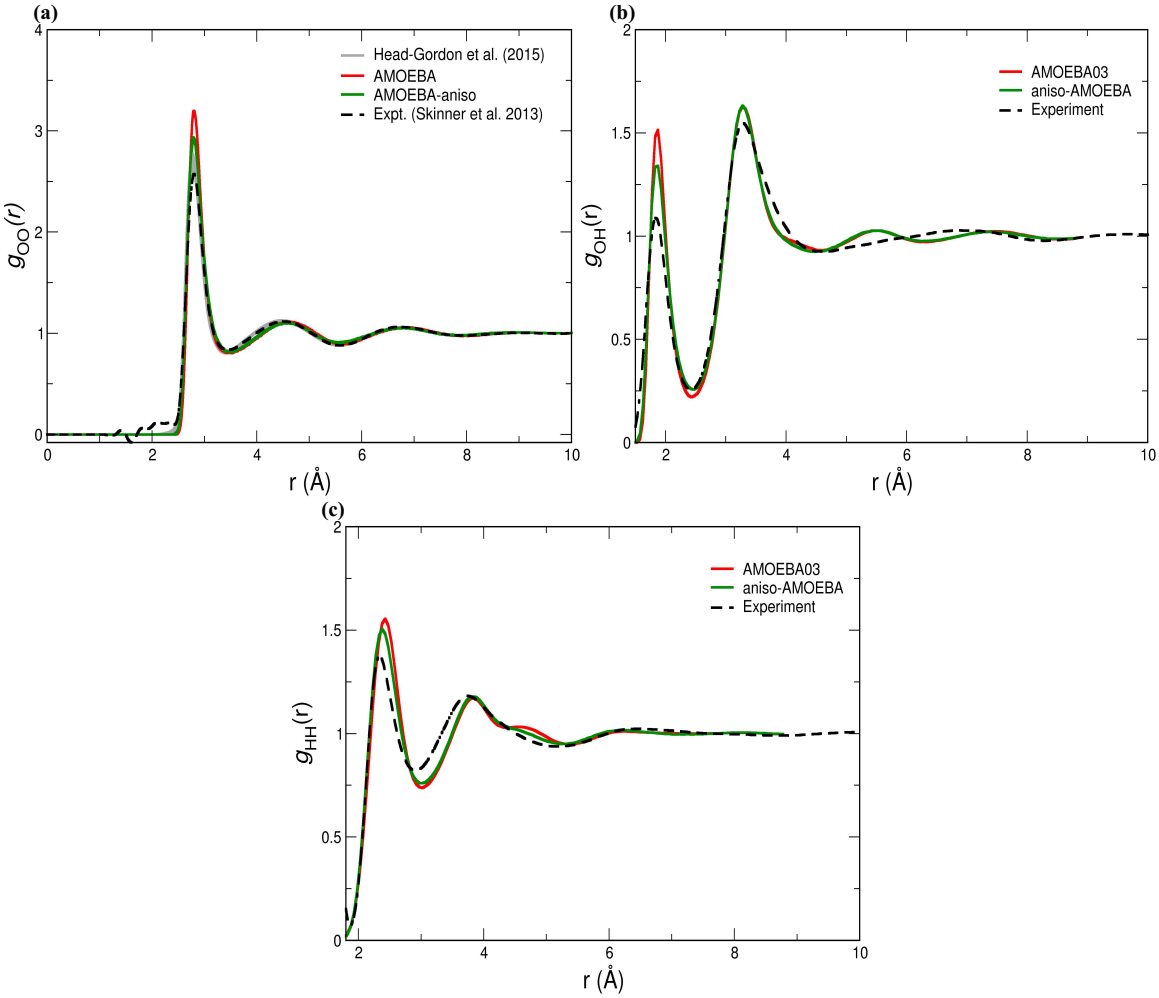

Figure 4. *Water radial distribution functions using aniso-AMOEBA and AMOEBA03 compared to experiment.* (a) $g_{OO}(r)$, (b) $g_{OH}(r)$, and (c) $g_{HH}(r)$. All simulations were performed at the experimental bulk liquid density at 300 K. The experimental data is shown as dashed line [72-73], while the additional aqua curves eliminates the

unphysical density at low *r* and conforms to the isothermal compressibility that overcomes problems with the original experimental analysis.[74]

The primary goal of the anisotropic water model is to improve energies and forces near the strongly asymmetric and polarizing environments around solutes and interfaces. Simple ions present a first good test where qualitatively we expect that anions will give rise to larger needs for anisotropy than cations. This is confirmed for the halogen Cl^- and Br^- anions which, like the water trimer, show substantial improvement in the polarization energy under the aniso-AMOEBA model compared to AMOEBA03. Figure 5 provides the results for both the $(H_2O)_2Cl^-$ and $H_2O(Cl^-)_2$ trimers in which the anisotropic polarization energy agrees far better with the polarization energy from the ALMO-EDA, not only around the equilibrium but also throughout the scanned distances (Figure 5a and 5b). This stems from reduction in the over-polarization and anti-cooperativity of the 2-body and 3-body polarization, respectively, compared to the isotropic AMOEBA03 model (Figure 5c-5f). Again, it is evident that both AMOEBA models are capturing substantial 3-body contributions from charge transfer. For the $(H_2O)_2Cl^-$ trimer, the total interaction energy at equilibrium using aniso-AMOEBA is underbound by 3.1 kJ/mol ($\sim k_bT$) while the isotropic AMOEBA model is overbound by 8.0 kJ/mol. Similar improved results are seen for the corresponding Br^- systems under the aniso-AMOEBA model relative to standard AMOEBA when compared to ALMO-EDA (Figure S1).

The polarization energy also improves significantly for the $(H_2O)_2F^-$ system compared to the isotropic AMOEBA model throughout the distance scan (Figure 6a), with evident better agreement in both the 2-body and 3-body polarization (Figure 6b and 6c). However, the total interaction energy is poorly described by both AMOEBA models due to evident problems with other intermolecular interactions, which we previously found was due to both van der Waals and permanent electrostatics that are far too unfavourable at short range[42]. Hence while the aniso-AMOEBA model corrects for the overpolarization of the standard AMOEBA result, it now exhibits significant underbinding near equilibrium for the total interaction energy. Furthermore, the results for $H_2O(F^-)_2$ remains abysmal for both AMOEBA models compared to the ALMO-EDA results (Figure S2); the water-ion distance for F^- is so small that it further exacerbates the classically treated electrostatics and crude approximation of Pauli repulsion of the AMOEBA models, thereby requiring as a minimum the incorporation of charge penetration to correct the qualitatively incorrect behaviour of the total interaction energy. This is clearly a necessary consideration for force field guidance by EDA that once a single decomposed term is corrected (such as the improvement of anisotropic polarization), other terms will need to be rebalanced.

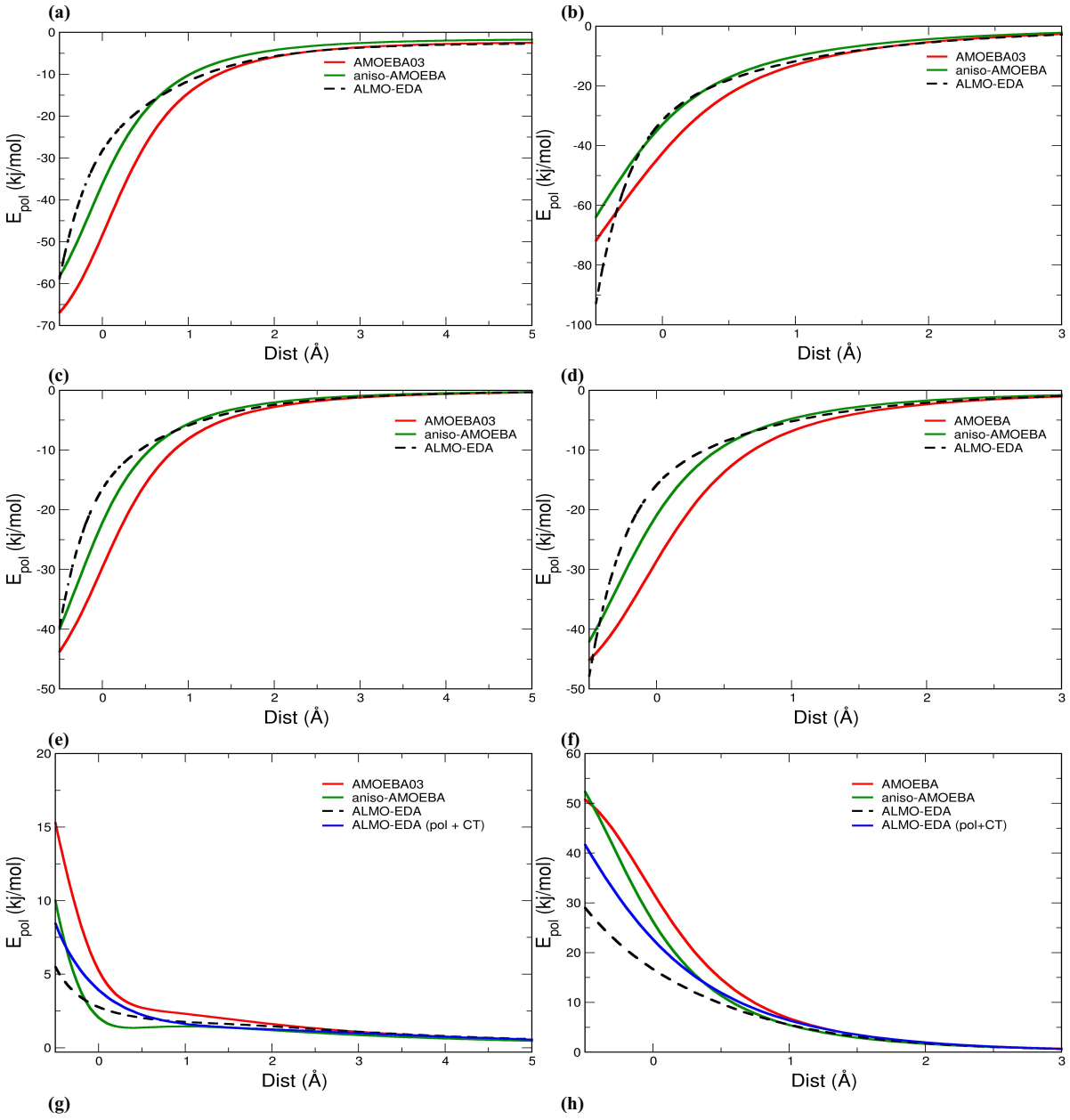
(a)
AMOEBA03
aniso-AMOEBA
ALMO-EDA
E_pol (kj/mol)
Dist (Å)
(b)
AMOEBA03
aniso-AMOEBA
ALMO-EDA
E_pol (kj/mol)
Dist (Å)
(c)
AMOEBA03
aniso-AMOEBA
ALMO-EDA
E_pol (kj/mol)
Dist (Å)
(d)
AMOEBA
aniso-AMOEBA
ALMO-EDA
E_pol (kj/mol)
Dist (Å)
(e)
AMOEBA03
aniso-AMOEBA
ALMO-EDA
ALMO-EDA (pol + CT)
E_pol (kj/mol)
Dist (Å)
(f)
AMOEBA
aniso-AMOEBA
ALMO-EDA
ALMO-EDA (pol+CT)
E_pol (kj/mol)
Dist (Å)
(g)
(h)

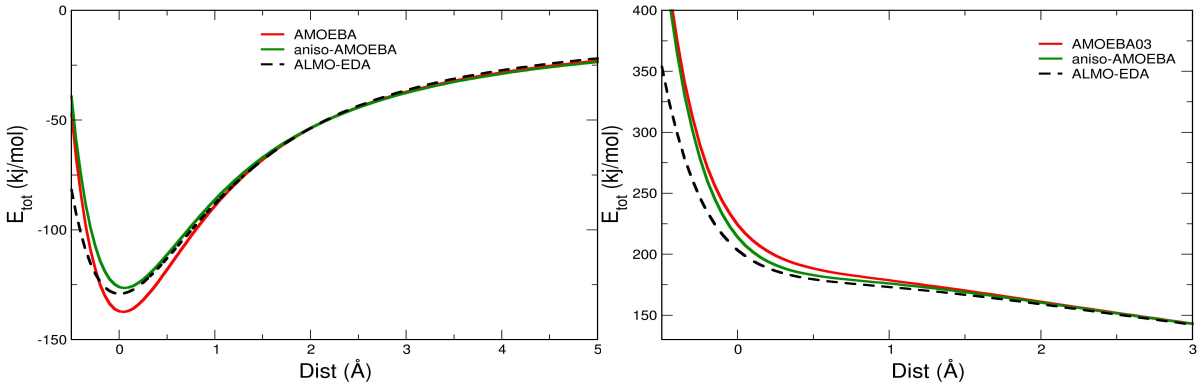

Figure 5. *Comparison of the aniso-AMOEBA (green) and standard AMOEBA model (red) when validated against ALMO-EDA (dashed) for $(H_2O)_2Cl^-$ (left column) and $H_2O(Cl^-)_2$ (right column) trimers*. (a-b) Total polarization energy, (c-d) 2-body polarization, (e-f) 3-body polarization compared to EDA polarization with and without charge transfer, (g-h) total interaction energy.

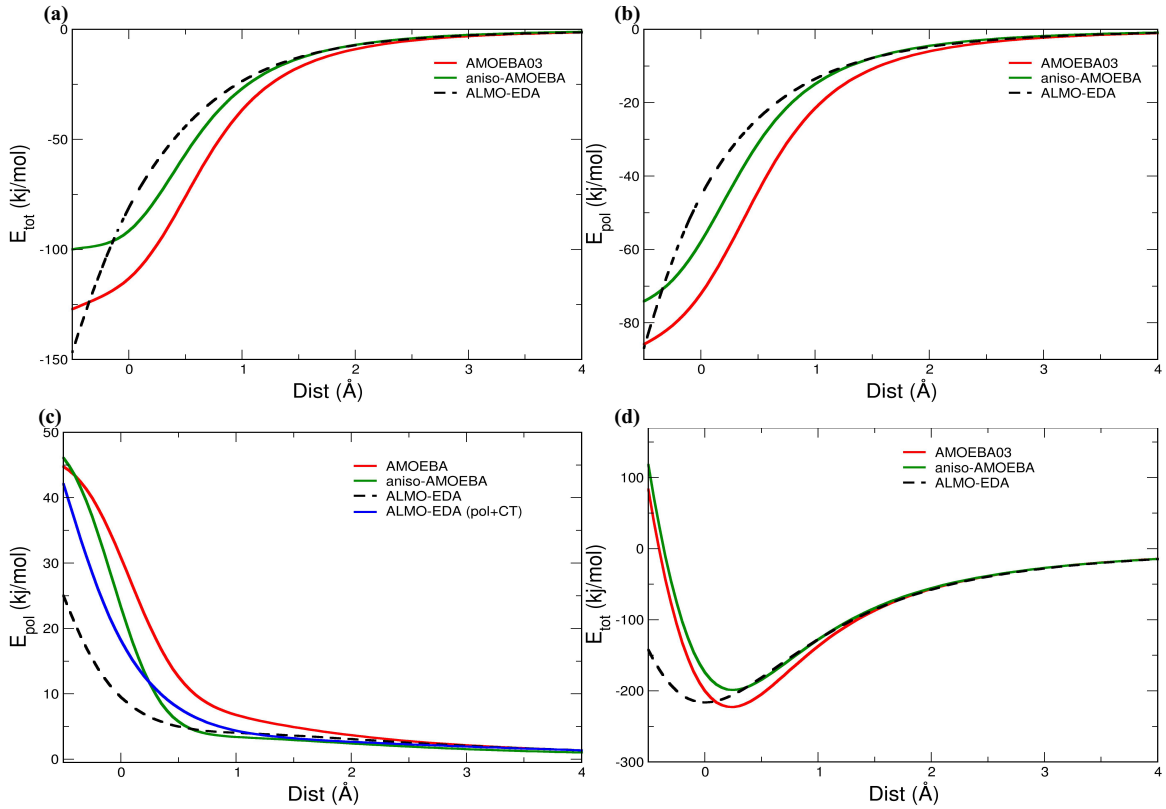

Figure 6. *Comparison of aniso-AMOEBA (green) and AMOEBA03 model (red) when validated against ALMO-EDA (dashed) for the $(H_2O)_2F^-$ trimer*. (a) Total polarization energy, (b) 2-body polarization, (c) 3-body polarization compared to EDA polarization with and without charge transfer (blue), (d) total interaction energy.

Unlike the halide ions, the anisotropic polarizability has a much smaller effect on the polarization energy for the single alkali and alkaline earth metal $(H_2O)_2M^{n+}$ systems, as expected. Given the small atomic radii, and therefore small polarizabilities of these cations, the isotropic polarizabilities are sufficient to describe their interactions with water (Figure 7 and S3-S6).[75] In all of

these cases both AMOEBA and aniso-AMOEBA consistently agree well with the ALMO-EDA polarization energy at equilibrium, while overestimating the polarization energy in the compressed region, and underestimating the polarization at larger separations. Therefore, the total interaction energy is very similar between the AMOEBA03 and aniso-AMOEBA models for the $(H_2O)_2M^{n+}$ systems. However, for the dication $H_2O(M^{n+})_2$ systems, there is a modest but clear trend that the larger the ion and the higher the net charge, the better is the polarization energy under the aniso-AMOEBA model. This trend originates in the qualitative improvement in capturing the greater anti-cooperative behaviour in the 3-body polarization as shown in Figure 8 for $H_2O(Ca^{2+})_2$ and supported in Figures S7-S10 for the corresponding Li^+, Na^+, K^+ and Mg^{2+} ions. We note that although ωB97X-V provides ~0.5 kcal/mol accuracy for almost all the investigated systems, it slightly overbinds the water-cation complexes in the long range due to self-interaction error, which is most pronounced in the $H_2O\cdots Mg^{2+}$ systems.

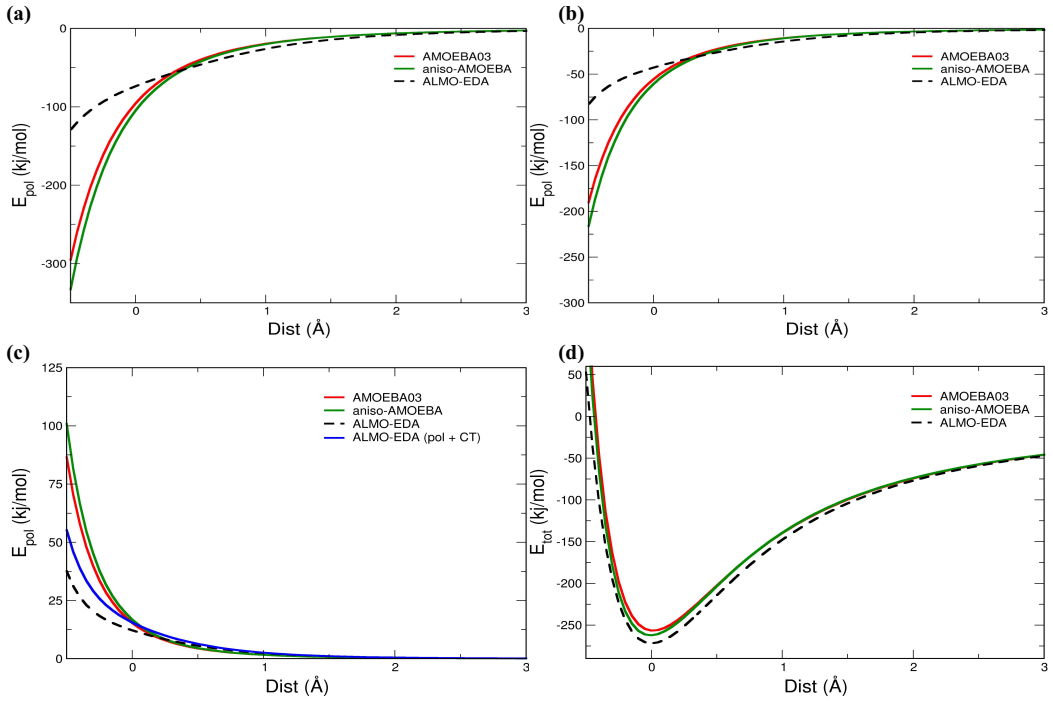

Figure 7. *Comparison of aniso-AMOEBA (green) and AMOEBA03 model (red) when validated against ALMO-EDA (dashed) for the $(H_2O)_2Li^+$ trimer.* (a) Polarization energy, (b) 2-body polarization, (c) 3-body polarization compared to EDA polarization with and without charge transfer, (d) total interaction energy.

(a) **(b)**

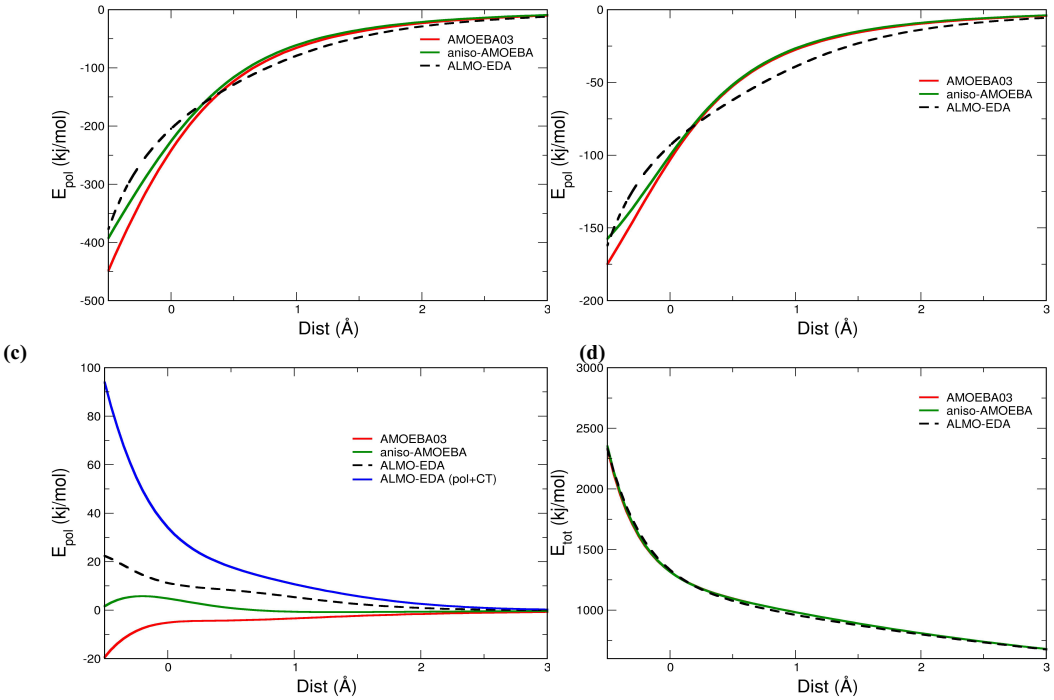

Figure 8. *Comparison of aniso-AMOEBA (green) and AMOEBA03 model (red) when validated against ALMO-EDA (dashed) for the $H_2O(Ca^{2+})_2$ trimer*. (a) Polarization energy, (b) 2-body polarization, (c) 3-body polarization compared to EDA polarization with and without charge transfer, (d) total interaction energy.

DISCUSSION AND CONCLUSION

In this work we have shown that the inclusion of anisotropic polarization for a single water molecule translates into noticeably improved polarization energy, and hence more accurate potential energy surfaces, across a wide range of systems including small and large gas phase water clusters, bulk water properties, and ionic clusters composed of monovalent and divalent ions complexed with one or two water molecules. For future considerations in reducing the computational cost, using only the diagonalized atomic polarizability matrix provides very similar results compared to full anisotropy for polarization for all trimer systems (Figure S11) near equilibrium, with most deviations occurring in the compressed regions for only a handful of systems. Even so, the computational cost of the full anisotropic matrix is only ~1.1 the cost of the standard isotropic model, and thus the small incurred errors through a reduced anisotropic model is not worthwhile in our view. Instead we believe that eliminating the self-consistent field steps using our extended Lagrangian formulation, as we have done for the isotropic AMOEBA model, should be easily extensible to aniso-AMOEBA to reduce the cost of a polarization model to that of permanent electrostatics only.[76-77] In summary, this study provides an excellent foundation for future work in which we will develop aniso-AMOEBA force fields for biologically relevant solutes like amino acids and DNA base pairs, or for complex materials

and interfaces, for prediction of properties for asymmetric environments where an accurate polarization model is most needed.

ACKNOWLEDGMENTS. We thank the National Science Foundation for support under Grant No CHE-1665315. This research used computational resources of the National Energy Research Scientific Computing Center, a DOE Office of Science User Facility supported by the Office of Science of the U.S. Department of Energy under Contract No. DE-AC02-05CH11231.

SUPPORTING INFORMATION. Water cluster binding energies and all distance scans and EDA analysis for ions not covered in main manuscript. Information is available free of charge via the Internet at http://pubs.acs.org.

REFERENCES

1. Karplus, M.; McCammon, J. A. Molecular dynamics simulations of biomolecules. *Nat. Struct. Biol.* **2002,** *9* (10), 788-788.
2. Childers, M. C.; Daggett, V. Insights from molecular dynamics simulations for computational protein design. *Mol. Syst. Des. Eng.* **2017,** *2* (1), 9-33.
3. Cheatham, I. I. I. T. E.; Case, D. A. Twenty-Five Years of Nucleic Acid Simulations. *Biopolymers* **2013,** *99* (12, SI), 969-977.
4. Zhang, C.; Lu, C.; Jing, Z.; Wu, C.; Piquemal, J.-P.; Ponder, J. W.; Ren, P. AMOEBA Polarizable Atomic Multipole Force Field for Nucleic Acids. *J. Chem. Theo. Comp.* **2018,** *14* (4), 2084-2108.
5. Laughton, C. A.; Harris, S. A. The atomistic simulation of DNA. *WIREs Comput. Mol. Sci.* **2011,** *1* (4), 590-600.
6. Baker, C. M. Polarizable force fields for molecular dynamics simulations of biomolecules. *WIREs Comput. Mol. Sci.* **2015,** *5* (2), 241-254.
7. Lopes, P. E. M.; Guvench, O.; MacKerell, J. A. D. Current Status of Protein Force Fields for Molecular Dynamics Simulations. In *Molecular Modeling of Proteins: 2nd Edition*, Kukol, A., Ed. 2015; Vol. 1215, pp 47-71.
8. Xuewei, L.; Danfeng, S.; Shuangyan, Z.; Hongli, L.; Huanxiang, L.; Xiaojun, Y. Molecular dynamics simulations and novel drug discovery. *Expert Opin. Drug Discov.* **2018,** *13* (1), 23-37.
9. Zhang, J.; Xu, F.; Hong, Y.; Xiong, Q.; Pan, J. A comprehensive review on the molecular dynamics simulation of the novel thermal properties of graphene. *RSC Adv.* **2015,** *5* (109), 89415-89426.
10. Demerdash, O.; Wang, L.-P.; Head-Gordon, T. Advanced models for water simulations. *Wiley Interdisciplinary Reviews: Computational Molecular Science* **2017,** *8* (1), e1355.
11. Nerenberg, P. S.; Head-Gordon, T. New developments in force fields for biomolecular simulations. *Curr Opin Struct Biol* **2018,** *49*, 129-138.
12. Huang, J.; Rauscher, S.; Nawrocki, G.; Ran, T.; Feig, M.; de Groot, B. L.; Grubmüller, H.; MacKerell Jr, A. D. CHARMM36m: an improved force field for folded and intrinsically disordered proteins. *Nat. Methods* **2016**.
13. Lane, T. J.; Shukla, D.; Beauchamp, K. A.; Pande, V. S. To milliseconds and beyond: challenges in the simulation of protein folding. *Curr. Opin. Struct. Biol.* **2013,** *23* (1), 58-65.

14. Piquemal, J.-P.; Chevreau, H.; Gresh, N. Toward a separate reproduction of the contributions to the Hartree-Fock and DFT intermolecular interaction energies by polarizable molecular mechanics with the SIBFA potential. *J. Chem. Theo. Comp.* **2007,** *3* (3), 824-837.
15. Lopes, P. E. M.; Huang, J.; Shim, J.; Luo, Y.; Li, H.; Roux, B.; MacKerell, J. A. D. Polarizable Force Field for Peptides and Proteins Based on the Classical Drude Oscillator. *J. Chem. Theo. Comp.* **2013,** *9* (12), 5430-5449.
16. Rappe, A. K.; Goddard, W. A. Charge Equilibration for Molecular-Dynamics Simulations. *J. Phys. Chem.* **1991,** *95* (8), 3358-3363.
17. Piquemal, J. P.; Cisneros, G. A.; Reinhardt, P.; Gresh, N.; Darden, T. A. Towards a force field based on density fitting. *J. Chem. Phys.* **2006,** *124* (10).
18. Cisneros, G. A.; Piquemal, J.-P.; Darden, T. A. Generalization of the Gaussian electrostatic model: Extension to arbitrary angular momentum, distributed multipoles, and speedup with reciprocal space methods. *J. Chem. Phys.* **2006,** *125* (18).
19. Ren, P. Y.; Ponder, J. W. Consistent treatment of inter- and intramolecular polarization in molecular mechanics calculations. *J. Comput. Chem.* **2002,** *23* (16), 1497-1506.
20. Shi, Y.; Xia, Z.; Zhang, J.; Best, R.; Wu, C.; Ponder, J. W.; Ren, P. Polarizable Atomic Multipole-Based AMOEBA Force Field for Proteins. *J. Chem. Theo. Comp.* **2013,** *9* (9), 4046-4063.
21. Ponder, J. W.; Wu, C.; Ren, P.; Pande, V. S.; Chodera, J. D.; Schnieders, M. J.; Haque, I.; Mobley, D. L.; Lambrecht, D. S.; DiStasio, J. R. A.; Head-Gordon, M.; Clark, G. N. I.; Johnson, M. E.; Head-Gordon, T. Current Status of the AMOEBA Polarizable Force Field. *J. Phys. Chem. B* **2010,** *114* (8), 2549-2564.
22. Lagardere, L.; Jolly, L. H.; Lipparini, F.; Aviat, F.; Stamm, B.; Jing, Z. F.; Harger, M.; Torabifard, H.; Cisneros, G. A.; Schnieders, M. J.; Gresh, N.; Maday, Y.; Ren, P. Y.; Ponder, J. W.; Piquemal, J. P. Tinker-HP: a massively parallel molecular dynamics package for multiscale simulations of large complex systems with advanced point dipole polarizable force fields. *Chem Sci* **2018,** *9* (4), 956-972.
23. Albaugh, A.; Boateng, H. A.; Bradshaw, R. T.; Demerdash, O. N.; Dziedzic, J.; Mao, Y.; Margul, D. T.; Swails, J.; Zeng, Q.; Case, D. A.; Eastman, P.; Wang, L.-P.; Essex, J. W.; Head-Gordon, M.; Pande, V. S.; Ponder, J. W.; Shao, Y.; Skylaris, C.-K.; Todorov, I. T.; Tuckerman, M. E.; Head-Gordon, T. Advanced Potential Energy Surfaces for Molecular Simulation. *J. Phys. Chem. B* **2016,** *120* (37), 9811-9832.
24. Albaugh, A.; Demerdash, O.; Head-Gordon, T. An efficient and stable hybrid extended Lagrangian/self-consistent field scheme for solving classical mutual induction. *J Chem Phys* **2015,** *143* (17), 174104.
25. Albaugh, A.; Head-Gordon, T. A New Method for Treating Drude Polarization in Classical Molecular Simulation. *J. Chem. Theo. Comp.* **2017,** *13* (11), 5207-5216.
26. Demerdash, O.; Mao, Y.; Liu, T.; Head-Gordon, M.; Head-Gordon, T. Assessing many-body contributions to intermolecular interactions of the AMOEBA force field using energy decomposition analysis of electronic structure calculations. *J. Chem. Phys.* **2017,** *147* (16).
27. Mobley, D. L.; Wymer, K. L.; Lim, N. M.; Guthrie, J. P. Blind prediction of solvation free energies from the SAMPL4 challenge. *J. Comput. Aided Mol. Des.* **2014,** *28* (3, SI), 135-150.
28. Mobley, D. L.; Liu, S.; Cerutti, D. S.; Swope, W. C.; Rice, J. E. Alchemical prediction of hydration free energies for SAMPL. *J. Comput. Aided Mol. Des.* **2012,** *26* (5, SI), 551-562.
29. Yin, J.; Henriksen, N. M.; Slochower, D. R.; Shirts, M. R.; Chiu, M. W.; Mobley, D. L.; Gilson, M. K. Overview of the SAMPL5 host-guest challenge: Are we doing better? *J. Comput. Aided Mol. Des.* **2017,** *31* (1, 2, SI), 1-19.

30. Bradshaw, R. T.; Essex, J. W. Evaluating Parametrization Protocols for Hydration Free Energy Calculations with the AMOEBA Polarizable Force Field. *J. Chem. Theo. Comp.* **2016,** *12* (8), 3871-3883.
31. Kitaura, K.; Morokuma, K. A new energy decomposition scheme for molecular interactions within the Hartree-Fock approximation. *International Journal of Quantum Chemistry* **1976,** *10* (2), 325-340.
32. Chen, W.; Gordon, M. S. Energy decomposition analyses for many-body interaction and applications to water complexes. *J. Phys. Chem.* **1996,** *100* (34), 14316-14328.
33. Mitoraj, M. P.; Michalak, A.; Ziegler, T. A Combined Charge and Energy Decomposition Scheme for Bond Analysis. *J. Chem. Theo. Comp.* **2009,** *5* (4), 962-975.
34. Su, P.; Li, H. Energy decomposition analysis of covalent bonds and intermolecular interactions. *J. Chem. Phys.* **2009,** *131* (1).
35. Reed, A. E.; Curtiss, L. A.; Weinhold, F. Intermolecular Interactions from a Natural Bond Orbital, Donor-Acceptor Viewpoint. *Chem. Rev.* **1988,** *88* (6), 899-926.
36. Schenter, G. K.; Glendening, E. D. Natural energy decomposition analysis: The linear response electrical self energy. *J. Phys. Chem.* **1996,** *100* (43), 17152-17156.
37. Jeziorski, B.; Moszynski, R.; Szalewicz, K. Perturbation-Theory Approach to Intermolecular Potential-Energy Surfaces of Van-der-Waals Complexes. *Chem. Rev.* **1994,** *94* (7), 1887-1930.
38. Misquitta, A. J.; Podeszwa, R.; Jeziorski, B.; Szalewicz, K. Intermolecular potentials based on symmetry-adapted perturbation theory with dispersion energies from time-dependent density-functional calculations. *J. Chem. Phys.* **2005,** *123* (21).
39. Khaliullin, R. Z.; Cobar, E. A.; Lochan, R. C.; Bell, A. T.; Head-Gordon, M. Unravelling the origin of intermolecular interactions using absolutely localized molecular orbitals. *J. Phys. Chem. A* **2007,** *111* (36), 8753-8765.
40. Horn, P. R.; Mao, Y.; Head-Gordon, M. Probing non-covalent interactions with a second generation energy decomposition analysis using absolutely localized molecular orbitals. *Phys. Chem. Chem. Phys* **2016,** *18* (33), 23067-23079.
41. Levine, D. S.; Horn, P. R.; Mao, Y.; Head-Gordon, M. Variational Energy Decomposition Analysis of Chemical Bonding. 1. Spin-Pure Analysis of Single Bonds. *J. Chem. Theo. Comp.* **2016,** *12* (10), 4812-4820.
42. Mao, Y.; Demerdash, O.; Head-Gordon, M.; Head-Gordon, T. Assessing Ion-Water Interactions in the AMOEBA Force Field Using Energy Decomposition Analysis of Electronic Structure Calculations. *J. Chem. Theo. Comp.* **2016,** *12* (11), 5422-5437.
43. Phipps, M. J. S.; Fox, T.; Tautermann, C. S.; Skylaris, C.-K. Energy decomposition analysis approaches and their evaluation on prototypical protein-drug interaction patterns. *Chem. Soc. Rev.* **2015,** *44* (10), 3177-3211.
44. Gordon, M. S.; Fedorov, D. G.; Pruitt, S. R.; Slipchenko, L. V. Fragmentation Methods: A Route to Accurate Calculations on Large Systems. *Chem. Rev.* **2012,** *112* (1), 632-672.
45. Mardirossian, N.; Head-Gordon, M. ωB97X-V: A 10-parameter, range-separated hybrid, generalized gradient approximation density functional with nonlocal correlation, designed by a survival-of-the-fittest strategy. *Phys. Chem. Chem. Phys* **2014,** *16* (21), 9904-9924.
46. Rappoport, D.; Furche, F. Property-optimized Gaussian basis sets for molecular response calculations. *J. Chem. Phys.* **2010,** *133* (13).
47. Ren, P. Y.; Ponder, J. W. Polarizable atomic multipole water model for molecular mechanics simulation. *J. Phys. Chem. B* **2003,** *107* (24), 5933-5947.
48. Thole, B. T. Molecular Polarizabilities Calculated with a Modified Dipole Interaction. *Chem. Phys.* **1981,** *59* (3), 341-350.

49. Jing, Z.; Qi, R.; Liu, C.; Ren, P. Study of interactions between metal ions and protein model compounds by energy decomposition analyses and the AMOEBA force field. *J. Chem. Phys.* **2017,** *147* (16).
50. Dudev, T.; Lim, C. Competition among Metal Ions for Protein Binding Sites: Determinants of Metal Ion Selectivity in Proteins. *Chem. Rev.* **2014,** *114* (1), 538-556.
51. Ponder, J. W.; Case, D. A. Force Fields for Protein Simulations. In *Protein Simulations*, Academic Press: 2003; Vol. 66, pp 27-85.
52. Thole, B. T. Molecular Polarizabilities Calculated with a Modified Dipole Interaction. *Chem Phys* **1981,** *59* (3), 341-350.
53. Misquitta, A. J.; Stone, A. J. CamCASP: a program for studying intermolecular interactions and for the calcula- tion of molecular properties in distributed form. *University of Cambridge, 2016*.
54. Stone, A. J.; Dullweber, A.; Engkvist, O.; Fraschini, E.; Hodges, M. P.; Meredith, A. W.; Nutt, D. R.; Popelier, P. L. A.; Wales, D. J. *Orient: A Program for Studying Interactions between Molecules*, 4.9; University of Cambridge: Cambridge, U.K., 2017.
55. Misquitta, A. J.; Stone, A. J. Distributed polarizabilities obtained using a constrained density-fitting algorithm. *The Journal of Chemical Physics* **2006,** *124* (2), 024111.
56. Misquitta, A. J.; Stone, A. J. Ab Initio Atom–Atom Potentials Using CamCASP: Theory and Application to Many-Body Models for the Pyridine Dimer. *Journal of Chemical Theory and Computation* **2016,** *12* (9), 4184-4208.
57. Valiev, M.; Bylaska, E. J.; Govind, N.; Kowalski, K.; Straatsma, T. P.; Van Dam, H. J. J.; Wang, D.; Nieplocha, J.; Apra, E.; Windus, T. L.; de Jong, W. A. NWChem: A comprehensive and scalable open-source solution for large scale molecular simulations. *Computer Physics Communications* **2010,** *181* (9), 1477-1489.
58. Misquitta, A. J.; Stone, A. J. Distributed polarizabilities obtained using a constrained density-fitting algorithm. *J. Chem. Phys.* **2006,** *124* (2).
59. Frisch, M. J.; Trucks, G. W.; Schlegel, H. B.; Scuseria, G. E.; Robb, M. A.; Cheeseman, J. R.; Scalmani, G.; Barone, V.; Mennucci, B.; Petersson, G. A.; Nakatsuji, H.; Caricato, M.; Li, X.; Hratchian, H. P.; Izmaylov, A. F.; Bloino, J.; Zheng, G.; Sonnenberg, J. L.; Hada, M.; Ehara, M.; Toyota, K.; Fukuda, R.; Hasegawa, J.; Ishida, M.; Nakajima, T.; Honda, Y.; Kitao, O.; Nakai, H.; Vreven, T.; Montgomery, J. J. A.; Peralta, J. E.; Ogliaro, F.; Bearpark, M.; Heyd, J. J.; Brothers, E.; Kudin, K. N.; Staroverov, V. N.; Kobayashi, R.; Normand, J.; Raghavachari, K.; Rendell, A.; Burant, J. C.; Iyengar, S. S.; Tomasi, J.; Cossi, M.; Rega, N.; Millam, J. M.; Klene, M.; Knox, J. E.; Cross, J. B.; Bakken, V.; Adamo, C.; Jaramillo, J.; Gomperts, R.; Stratmann, R. E.; Yazyev, O.; Austin, A. J.; Cammi, R.; Pomelli, C.; Ochterski, J. W.; Martin, R. L.; Morokuma, K.; Zakrzewski, V. G.; Voth, G. A.; Salvador, P.; Dannenberg, J. J.; Dapprich, S.; Daniels, A. D.; Farkas, O.; Foresman, J. B.; Ortiz, J. V.; Cioslowski, J.; Fox, D. J. Gaussian09 Revision D.01. 2009.
60. Horn, P. R.; Mao, Y.; Head-Gordon, M. Defining the contributions of permanent electrostatics, Pauli repulsion, and dispersion in density functional theory calculations of intermolecular interaction energies. *J. Chem. Phys.* **2016,** *144* (11).
61. Demerdash, O.; Mao, Y.; Liu, T.; Head-Gordon, M.; Head-Gordon, T. Assessing many-body contributions to intermolecular interactions of the AMOEBA force field using energy decomposition analysis of electronic structure calculations. *J Chem Phys* **2017,** *147* (16), 161721.
62. Shao, Y.; Gan, Z.; Epifanovsky, E.; Gilbert, A. T. B.; Wormit, M.; Kussmann, J.; Lange, A. W.; Behn, A.; Deng, J.; Feng, X.; Ghosh, D.; Goldey, M.; Horn, P. R.; Jacobson, L. D.; Kaliman, I.; Khaliullin, R. Z.; Kus, T.; Landau, A.; Liu, J.; Proynov, E. I.; Rhee, Y. M.; Richard, R. M.; Rohrdanz, M. A.; Steele, R. P.; Sundstrom, E. J.; Woodcock, I. I. I. H. L.; Zimmerman, P. M.; Zuev, D.; Albrecht, B.; Alguire, E.; Austin, B.; Beran, G. J. O.; Bernard, Y. A.; Berquist, E.; Brandhorst, K.; Bravaya, K. B.; Brown, S. T.; Casanova, D.; Chang, C.-M.; Chen, Y.; Chien, S. H.;

Closser, K. D.; Crittenden, D. L.; Diedenhofen, M.; DiStasio, J. R. A.; Do, H.; Dutoi, A. D.; Edgar, R. G.; Fatehi, S.; Fusti-Molnar, L.; Ghysels, A.; Golubeva-Zadorozhnaya, A.; Gomes, J.; Hanson-Heine, M. W. D.; Harbach, P. H. P.; Hauser, A. W.; Hohenstein, E. G.; Holden, Z. C.; Jagau, T.-C.; Ji, H.; Kaduk, B.; Khistyaev, K.; Kim, J.; Kim, J.; King, R. A.; Klunzinger, P.; Kosenkov, D.; Kowalczyk, T.; Krauter, C. M.; Lao, K. U.; Laurent, A. D.; Lawler, K. V.; Levchenko, S. V.; Lin, C. Y.; Liu, F.; Livshits, E.; Lochan, R. C.; Luenser, A.; Manohar, P.; Manzer, S. F.; Mao, S.-P.; Mardirossian, N.; Marenich, A. V.; Maurer, S. A.; Mayhall, N. J.; Neuscamman, E.; Oana, C. M.; Olivares-Amaya, R.; OŃeill, D. P.; Parkhill, J. A.; Perrine, T. M.; Peverati, R.; Prociuk, A.; Rehn, D. R.; Rosta, E.; Russ, N. J.; Sharada, S. M.; Sharma, S.; Small, D. W.; Sodt, A.; Stein, T.; Stueck, D.; Su, Y.-C.; Thom, A. J. W.; Tsuchimochi, T.; Vanovschi, V.; Vogt, L.; Vydrov, O.; Wang, T.; Watson, M. A.; Wenzel, J.; White, A.; Williams, C. F.; Yang, J.; Yeganeh, S.; Yost, S. R.; You, Z.-Q.; Zhang, I. Y.; Zhang, X.; Zhao, Y.; Brooks, B. R.; Chan, G. K. L.; Chipman, D. M.; Cramer, C. J.; Goddard, I. I. I. W. A.; Gordon, M. S.; Hehre, W. J.; Klamt, A.; Schaefer, I. I. I. H. F.; Schmidt, M. W.; Sherrill, C. D.; Truhlar, D. G.; Warshel, A.; Xu, X.; Aspuru-Guzik, A.; Baer, R.; Bell, A. T.; Besley, N. A.; Chai, J.-D.; Dreuw, A.; Dunietz, B. D.; Furlani, T. R.; Gwaltney, S. R.; Hsu, C.-P.; Jung, Y.; Kong, J.; Lambrecht, D. S.; Liang, W.; Ochsenfeld, C.; Rassolov, V. A.; Slipchenko, L. V.; Subotnik, J. E.; Van Voorhis, T.; Herbert, J. M.; Krylov, A. I.; Gill, P. M. W.; Head-Gordon, M. Advances in molecular quantum chemistry contained in the Q-Chem 4 program package. *Mol. Phys.* **2015,** *113* (2), 184-215.

63. Laury, M. L.; Wang, L. P.; Pande, V. S.; Head-Gordon, T.; Ponder, J. W. Revised Parameters for the AMOEBA Polarizable Atomic Multipole Water Model. *J. Phys. Chem. B* **2015,** *119*, 9423.

64. Clough, S. A.; Beers, Y.; Klein, G. P.; Rothman, L. S. Dipole-Moment of Water from Stark Measurements of H2O, HDO, and D2O. *Journal of Chemical Physics* **1973,** *59*, 2254-2259.

65. Verhoeven, J.; Dymanus, A. Magnetic Properties and Molecular Quadrupole Tensor of the Water Molecule by Beam-Maser Zeeman Spectroscopy. *Journal of Chemical Physics* **1970,** *52*, 3222-3233.

66. Murphy, W. F. The Rayleigh Depolarization Ratio and Rotational Raman Spectrum of Water Vapor and the Polarizability Components for the Water Molecule. *Journal of Chemical Physics* **1977,** *67*, 5877-5882.

67. Curtiss, L. A.; Frurip, D. J.; Blander, M. Studies of Molecular Association in H2O and D2O Vapors by Measurement of Thermal Conductivity. *Journal of Chemical Physics* **1979,** *71*, 2703-2711.

68. Odutola, J. A.; Dyke, T. R. Partially Deuterated Water Dimers - Microwave-Spectra and Structure. *J. Chem. Phys.* **1980,** *72*, 5062-5070.

69. Tschumper, G. S.; Leininger, M. L.; Hoffman, B. C.; Valeev, E. F.; Schaefer, H. F.; Quack, M. Anchoring the Water Dimer Potential Energy Surface with Explicitly Correlated Computations and Focal Point Analyses. *Journal of Chemical Physics* **2002,** *116*, 690-701.

70. Klopper, W.; van Duijneveldt-van de Rijdt, J. G. C. M.; van Duijneveldt, F. B. Computational Determination of Equilibrium Geometry and Dissociation Energy of the Water Dimer. *Physical Chemistry Chemical Physics* **2000,** *2*, 2227-2234.

71. Lee, H. M.; Suh, S. B.; Lee, J. Y.; Tarakeshwar, P.; Kim, K. S. Structures, Energies, Vibrational Spectra, and Electronic Properties of Water Monomer to Decamer. *Journal of Chemical Physics* **2000,** *112*, 9759-9772.

72. Skinner, L. B.; Huang, C.; Schlesinger, D.; Pettersson, L. G.; Nilsson, A.; Benmore, C. J. Benchmark oxygen-oxygen pair-distribution function of ambient water from x-ray diffraction measurements with a wide Q-range. *J Chem Phys* **2013,** *138* (7), 074506.

73. Soper, A. K. The Radial Distribution Functions of Water as Derived from Radiation Total Scattering Experiments: Is There Anything We Can Say for Sure? *ISRN Physical Chemistry* **2013,** *2013*, 279463.
74. Brookes, D. H.; Head-Gordon, T. Family of Oxygen–Oxygen Radial Distribution Functions for Water. *The Journal of Physical Chemistry Letters* **2015,** *6* (15), 2938-2943.
75. Trumm, M. On the Isotropy of Induced Multipole Moments in Heavy Ion Complexes. *J. Comput. Chem.* **2018,** *39* (7), 373-379.
76. Albaugh, A.; Demerdash, O.; Head-Gordon, T. An efficient and stable hybrid extended Lagrangian/self-consistent field scheme for solving classical mutual induction. *The Journal of Chemical Physics* **2015,** *143* (17), 174104.
77. Albaugh, A.; Niklasson, A. M. N.; Head-Gordon, T. Accurate Classical Polarization Solution with No Self-Consistent Field Iterations. *The Journal of Physical Chemistry Letters* **2017,** *8* (8), 1714-1723.